Computer Methods and Programs in Biomedicine 163 (2018) 155–168

Contents lists available at ScienceDirect

Computer Methods and Programs in Biomedicine

journal homepage: www.elsevier.com/locate/cmpb

State-of-the-art review on automated lumen and adventitial border delineation and its measurements in carotid ultrasound

P Krishna Kumar[a], Tadashi Araki[b], Jeny Rajan[c], John R Laird[d], Andrew Nicolaides[e], Jasjit S. Suri[f,g,*], Fellow AIMBE

[a] Department of Computer Science and Engineering, National Institute of Technology Calicut, Kerala, India
[b] Division of Cardiovascular Medicine, Toho University Ohashi Medical Center, Tokyo, Japan
[c] Department of Computer Science and Engineering, National Institute of Technology Karnataka, Surathkal, India
[d] Heart and Vascular Institute, Adventist Health, St. Helena, CA, USA
[e] Vascular Diagnostic Center, University of Cyprus, Nicosia, Cyprus
[f] Stroke Monitoring Division, AtheroPoint, Roseville, CA, USA
[g] Department of Electrical Engineering, University of Idaho (Affl.), ID, USA

ARTICLE INFO

Article history:
Received 12 September 2017
Revised 29 April 2018
Accepted 9 May 2018

Keywords:
Carotid artery
Stenosis
B-mode ultrasound
Lumen diameter
Inter-adventitial diameter
Segmentation
Measurement
Performance

ABSTRACT

Background and objective: Accurate, reliable, efficient, and precise measurements of the lumen geometry of the common carotid artery (CCA) are important for (a) managing the progression/regression of atherosclerotic build-up and (b) the risk of stroke. The image-based degree of stenosis in the carotid artery and the plaque burden can be predicted using the automated carotid lumen diameter (LD)/inter-adventitial diameter (IAD) measurements from B-mode ultrasound images. The objective of this review is to present the state-of-the-art methods and systems for the measurement of LD/IAD in CCA based on automated or semi-automated strategies. Further, the performance of these systems is compared based on various metrics for its measurements.

Methods: The automated algorithms proposed for the segmentation of carotid lumen are broadly classified into two different categories as: region-based and boundary-based. These techniques are discussed in detail specifying their pros and cons. Further, we discuss the challenges encountered in the segmentation process along with its quantitative assessment. Lastly, we present stenosis quantification and risk stratification strategies.

Results: Even though, we have found more boundary-based approaches compared to region-based approaches in the literature, however, the region-based strategy yield more satisfactory performance. Novel risk stratification strategies are presented. On a patient database containing 203 patients, 9 patients are identified as high risk patients, whereas 27 patients are identified as medium risk patients.

Conclusions: We have presented different techniques for the lumen segmentation of the common carotid artery from B-mode ultrasound images and measurement of lumen diameter and inter-adventitial diameter. We believe that the issue regarding boundary-based techniques can be compensated by taking regional statistics embedded with boundary-based information.

1. Introduction

Stroke is the second leading cause of disability among adults worldwide, after dementia [1]. Recent reports show that approximately 795,000 people suffer from stroke each year and nearly 75% of these occur in people over the age of 65 [2]. Stroke occurs either when (a) the blood supply to the brain is blocked due to carotid stenosis or (b) the sudden rupture of a blood vessel within the brain leading to blockages [3]. The former one is called as ischemic stroke and the latter is called as hemorrhagic stroke. Stroke causes severe and permanent damage to the brain and affects the cognitive functioning [4].

Carotid stenosis is a progressive narrowing of the carotid arteries caused by a build-up of plaque (atherosclerosis) inside the artery wall which inhibits smooth blood flow. Plaque is a sticky substance made of lipid, cholesterol, calcium, and other fibrous materials [5]. Over time, plaque deposits inside the inner wall of the artery and can form a large mass that narrows the lumen, the inside diameter of the artery. The degree of luminal narrow-

* Corresponding author at: Monitoring and Diagnostic Division, AtheroPoint™, Roseville, CA, USA.
E-mail address: jasjit.suri@atheropoint.com (J.S. Suri).

https://doi.org/10.1016/j.cmpb.2018.05.015
0169-2607/

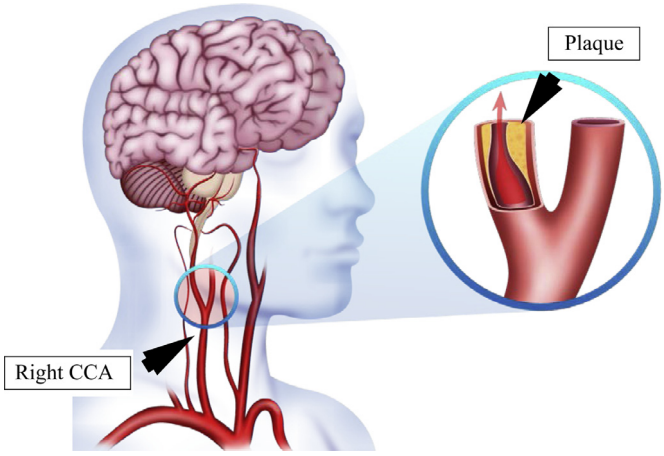

Fig. 1. Illustrates a blockage lodged in a blood vessel (Courtesy of AtheroPoint™, Roseville, CA, USA).

ing is considered as an indirect measure of the stenosis severity due to carotid atherosclerosis [6]. Continuous monitoring of these changes in the carotid lumen is therefore crucial in patient's diagnosis. Fig. 1 illustrates the blockage lodged in the common carotid artery (CCA) leading to stroke.

Different imaging techniques (computed tomography (CT), magnetic resonance imaging (MRI), ultrasound (US), digital subtraction angiography (DSA) etc.) have long been used for the accurate evaluation and treatment of carotid artery diseases. Out of these, US imaging is a widely accepted technique for its inherent advantages such as low cost, non-invasiveness, no radiation and portability [7]. Further, the US examination can be performed in patients with pacemakers or spinal stimulators. Hence, US imaging carries an important role in the effective management of patients with carotid artery disease. There are two main types of US imaging currently in use for the diagnosis of carotid artery. One is B-mode ultrasound imaging which aids in the visualization and measurement of the carotid arterial morphology [8]. Doppler US imaging is another standard clinical tool for the assessment of hemodynamics of carotid artery [9].

Color Doppler US provides information regarding blood flow in the lumen, which enables the clinician to detect flow reduction, flow turbulence and occlusion in arteries [10]. However, Doppler ultrasound may not be able to give a clear picture of the stenosis since the blood velocity is not constant [11]. Moreover, the Doppler spectrum is likely to get distorted (Doppler mismatch) by an acoustic impedance mismatch between the fluid and the vessel walls [12]. This mismatch is more prevalent in case of patients with hypotension or hypertension, tortuous vessels, presence of hypoechoic or calcified plaques and pre-occlusive lesion [13]. The image-based disease diagnosis technique (e.g. B-mode ultrasound) does not depend on blood velocity; rather, capturing the morphology of the plaque build-up is purely based on the reflection of sound. Therefore, it has a better chance of determining the severity of atherosclerosis disease. Fig. 2 illustrates the standardized approach for carotid ultrasound scanning [14].

The lumen diameter (LD)/inter-adventitial diameter (IAD) of the CCA, measured from B-mode US images can be considered as a surrogate marker for the risk of cardiovascular diseases (CVDs). Fig. 3 illustrates the lumen-intima (LI) and media-adventitia (MA) interfaces in an ultrasound image. LD is measured as the average distance between the two LI interfaces (distal and proximal) and similarly IAD is measured as the average distance between the two MA interfaces. An increase in the IAD or decrease in the LD has been correlated with the incident of stroke events [15]. The

Fig. 2. Meijer Carotid Arc: illustrates the standardized approach for carotid ultrasound scanning which will give a set of reproducible images (Reprinted from Stein et al. [14], license number 4184820134379 (Sep 2017), with permission from Elsevier).

CCA diameter has shown to be correlated to cardiac events [16], age [17], and other conventional vascular risk factors like gender, smoking history, hyperlipidemia, and hypertension [18,19]. Further, the carotid IAD is independently associated with first-time incident ischemic stroke, left ventricular mass and intima-media thickness (IMT) [20,21]. Moreover, the plaque formation in the carotid artery is an early indicator for coronary artery disease and myocardial infarction (MI) [22]. The asymptomatic carotid artery stenosis can be quantified by measuring the changes in the LD/IAD over time, and can be used as a secondary validated measure to decide whether carotid endarterectomy/stenting is required or not. The ability to provide reliable, accurate and highly reproducible measurements makes LD/IAD an attractive imaging biomarker.

A large number of follow-up studies have been used high-resolution B-mode ultrasonography to investigate the determinants of atherosclerotic disease, because of its ability to identify the atherosclerotic lesions at all stages of development [23,24]. Usually, delineation of the CCA are performed manually by medical experts using calipers [25], but it was shown that this process is tedious, prone to errors, and has large observer variability [26,27]. Further, the real time imaging of carotid artery is now possible due to the availability of better image reconstruction tools in ultrasound imaging (e.g. compound and harmonic imaging [25,28] and emerging super harmonic imaging [29]). However, automated methods are required for the accurate and reliable delineation of the CCA and measurement of the LD/IAD.

There are several challenges for the automated carotid lumen segmentation from US images and the measurement of LD/IAD. These are primarily due to the variability in size and shape of the artery, presence of plaque and curvature in arteries [25,28,30–31]. Since there is variation in image contrast due to plaque composition, stage and grade of the deposited plaque at the lumen-wall interface [32], the threshold-based systems often fail in segmenting the artery. High level of speckle content is another important

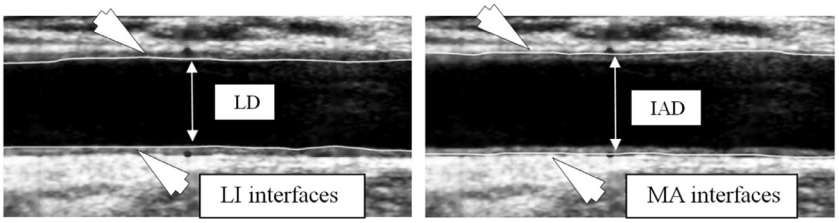

Fig. 3. Illustrates the (a) lumen-intima (LI) and (b) media-adventitia (MA) interfaces in an ultrasound image.

factor which poses a challenge in the automated segmentation process compromising the accuracy [30]. In this review, we considered only those techniques that are designed for segmenting the entire carotid lumen and that can be used to measure LD/IAD. Note that, the scope of the study is only towards segmentation of lumen and adventitial interfaces and measurements of LD/IAD. Further, it should be noted that the scope is not the review on IMT region segmentation and its measurement.

A more comprehensive assessment of predictors of CVD events such as LD/IAD could finally lead to an optimal treatment. Therefore, it is the aim of this review to give an overview about the state-of-the-art techniques in carotid lumen segmentation and the concepts regarding the carotid/coronary artery risk predictors. In Section 2, we present different CCA segmentation techniques, challenges in the segmentation methods in detail, and different measures used for the quantitative assessment of different segmentation systems including statistical tests. In Section 3, we discuss clinical significance of carotid LD and IAD and novel risk stratification strategies are presented along with analysis results. We discuss about the recent trends in the carotid artery segmentation, data analysis and validation process in Section 4. Finally, Section 5 concludes and outlines unsolved challenges in CCA ultrasound image segmentation.

2. Methods

2.1. Carotid lumen segmentation techniques

Accurate knowledge and understanding of the geometry of the carotid artery is important in their segmentation. Several automated algorithms have been proposed for the segmentation of the carotid lumen, but majority of them are focused on the segmentation and measurement of IMT. However, a few authors have pointed out the need for automated measurement of carotid LD [33–35]. The lumen segmentation algorithms can be broadly classified into two different categories as: region-based [36–40] and boundary-based [40–46]. The class of segmentation algorithms in image processing is based on two properties, similarity and discontinuity. The region-based model works by assuming constant intensity or similarity throughout a specific region which follows from the constant blood density assumption [47,48]. Since no gradient information is used in the process, the segmentation will be robust to cases having discontinuity in the boundaries of the carotid artery. Unlike region-based methods, the boundary-based approaches generally follow parametric curves (traditional snakes) or geometric curves (level set) with a manual initialization. Moreover, since boundary-based approaches rely on intensity gradients (intensity discontinuity), they are often susceptible to false edges or bleeding in the lumen borders [49,50]. Fig. 4 shows a general flow diagram of region-based and boundary-based lumen segmentation. Each of these steps is analyzed in detail in coming sections.

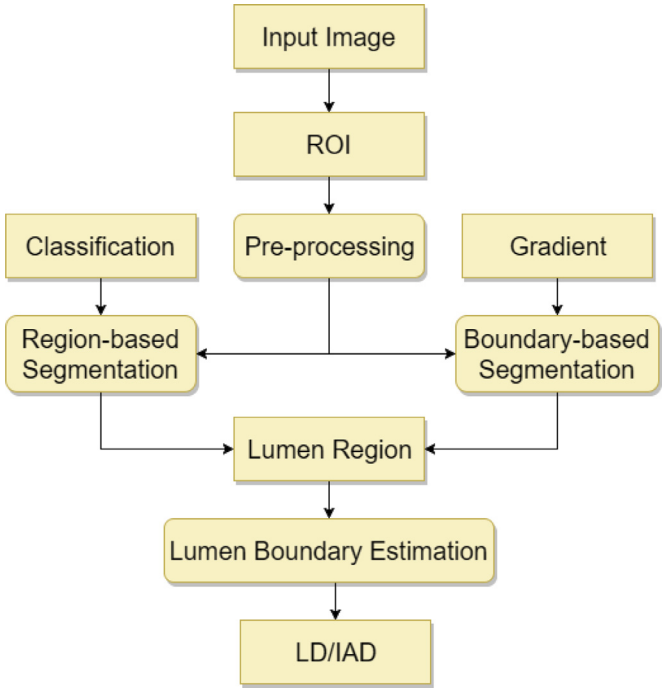

Fig. 4. General flow diagram showing the region-based and boundary-based carotid lumen segmentation.

2.1.1. Region of interest selection

In most of the studies, the segmentation is designed as a two stage process. Recognition of the region of interest (ROI) around the carotid artery is considered as the first stage. Tracing of the LI boundaries is the second stage. Commonly, the region between the outer wall layers (near adventitia layer and the far adventitia layer) is taken as ROI. This provides many advantages while tracing the LI interfaces. First of all, the CCA can be easily confounded with the jugular vein (JV) because their echo graphic appearance is very similar. Then, while considering the morphological aspect of the CCA, the artery can be of different shape and straight or curved. However, once we select the ROI, we have only limited area to search for the LI interfaces.

Golemati et al. [42] presented an algorithm that define four specific points to describe the ROI. Morphological opening is performed on the original image followed by binarization with a suitable threshold. Then four border points were defined based on the first and last pixel with a value one along the row and column. However, this algorithm has limitations in less bright images where a portion of the lumen region may get removed in the process. Rocha et al. [45] have chosen the ROI as the smallest rectangular box containing all pixels within a fixed distance from the user defined lumen axis. This distance is estimated based on the lumen width of the largest carotid artery image found in the database (approximately 70–90 pixels). Even though this seems reasonable, since it gives a good safety margin for rest of the images, sometimes it may produce unsatisfactory results.

In another automatic approach [46], classical Otsu's algorithm was used to compute two different thresholds, T_1 and T_2, and a

binary image is generated which contains only the objects having intensity in between T_1 and T_2 (assuming adventitial region comes within this intensity range). After removing smaller objects (text or graphical markings) using morphological opening, ROI is then defined as the smallest rectangle that encloses the lumen and adventitia regions. Sifakis et al. [36] used an approach to recognize the potential ROIs where they used user-defined percentile-based thresholds for local mean and variance of vertical intensities. Even though threshold based methods are able to remove texts and graphical markings, the area covered by the ROI need to be further reduced in order to increase the accuracy of segmentation.

Araki et al. [40] used a scale-space framework combined with vertical intensity profile analysis to find the ROI. Each column of the image pixels has been analysed from bottom to top and identified the pair of peaks corresponding to the adventitial borders (MA borders). The region between the two MA borders is then selected as the ROI. We believe that this is the best approximation for ROI as far as LD/IAD measurement is concerned and cannot reduce further.

2.1.2. Pre-processing

Once we compute the ROI, the next step is to do some pre-processing to enhance the images. This helps in improving the quality of image in ways that increase the accuracy of segmentation. Some authors have performed a Gaussian smoothing [37, 42, 44] or speckle filtering [41,43] of ROI. This is to reduce the noise in the image and thereby easing the process of LI interface detection. In [41], the image is processed with the application of an anisotropic diffusion filter for speckle removal prior to segmentation. Similarly in [43], the authors have used the linear scaling filter (despeckle filter linear scaling mean variance-DsFlsmv) to reduce the multiplicative noise prior to the segmentation. A Non-linear smoothing filter was conceived in [45] and applied to the ROI to reduce the noise before computing the edge map.

In [44], the speckle noise has attenuated by convolving the image with a Gaussian low pass filter. In Gaussian filters, the amount of smoothing is controlled by the standard deviation (σ) of the kernel, the value of which must be significant to reduce the noise present in images. However, if it is too large, it can result in complete blurring of the CCA walls. The carotid lumen images of CVD patients usually contain protruding hypoechogenic plaques. Further, the low contrast of the LI interfaces is another reason why we need to select an optimal value for σ. Thus, the selected value should be the one that offers a good compromise between noise removal and prevention of incursions. For example, in [37], the authors have chosen σ value of 1.2 mm, whereas in [44], σ value is set to 20 pixels (approximately 1.25 mm based on the image resolution). Morphological closing was performed as a pre-processing step in Golemati et al. [42] to merge small “channels” and “openings” of the image. Here, the shape and size of the structuring element is selected such that it does not alter the anatomical information contained in the image.

The next step after pre-processing is the segmentation. As stated earlier, the segmentation algorithms in the literature can be broadly classified into two: region-based and boundary-based, which are discussed below and their merits/demerits are compared in detail.

2.1.3. Region-based techniques

The region-based model works based on the distribution of image intensities and hence able to capture the lumen area under the constant blood density assumption [47]. There exist only a few region-based methods in the literature which are summarized in Table 1 along with performance statistics and limitations. These limitations are an indication of future research perspectives.

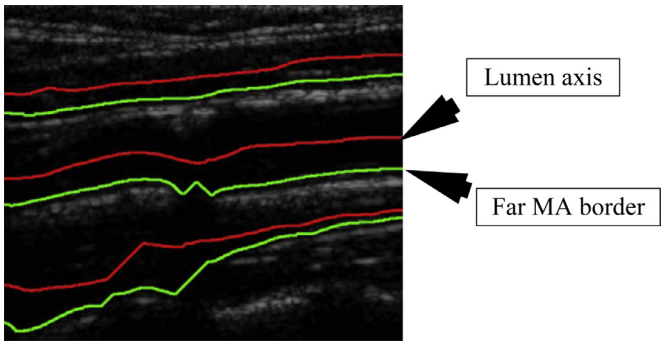

Fig. 5. Paths of local minima (red curves) and paths of local maxima (green curves) (Reprinted from Rocha et al. [37], license number 4,307,550,770,341 (March 2018), with permission from Elsevier). (For interpretation of the references to color in this figure legend, the reader is referred to the web version of this article.)

A sub-pixel resolution method was suggested by Cinthio et al. [38] for carotid LD measurement which utilizes relative threshold detection on the arterial walls. The grayscale information was averaged laterally within a pre-defined ROI to produce an envelope profile. Then, the vessel wall edges were found out by applying a suitable threshold which was determined based on the maximum intensity points in the profile. The process is repeated again after increasing the image resolution to get the refined positions of the walls. The threshold values were determined relative to the maximum level of the echo which can vary from person to person (approximately 20% at the near wall and 10% at the far wall). Even though this method reduces the computational load by giving a more robust estimate for sub-optimal images, a major problem is regarding with the underestimation of the LD. Further, the assumption of horizontal orientation is not an apt choice for the carotid artery, since arteries may appear tortuous or tilted depending on the acquisition.

Sifakis et al. [36] made an attempt to find the carotid lumen center points based on the distributions of local mean and variance of image intensities. A candidate point will be classified as a lumen pixel only if their corresponding local mean intensity and variance distribution belongs to its lower quartile. The authors have made an assumption that a majority of these points (potential lumen center points) will be found in a similar depth within the US image. This depth is identified by comparing the local depth level with a step-wisely decreasing threshold value of 2 mm. In this way, the algorithm effectively localizes the carotid artery lumen with relatively low computational cost. However, relatively low performance was observed in certain cases. Though the authors have addressed the carotid lumen segmentation problem, there was no discussion about the quantification of LD or IAD. Hence, we did not include the performance statistics of [36] in Table 1.

Rocha et al. [37] used a linear Bayes classifier to classify a set of longitudinal paths in the process of locating the carotid lumen axis. These paths are identified under the assumption that a sequence of local minima of smoothed ROI will appear near the lumen axis of blood vessels (indicated in red in Fig. 5) and a sequence of local maxima of the gradient magnitude of ROI will appear near the far wall of each vessel (indicated in green in Fig. 5). Then the dynamic programming (DP) algorithm is used to determine the actual longitudinal paths using a cost map. Any pair of adjacent red and green paths, such that green path is below the red one, are possible estimates of the lumen axis (This will be true only when the red path indicates the lumen axis and the green path indicates the far MA border). The authors have claimed that the method is not misguided by the JV above the CCA or vessel-like structures below the CCA. However, this method cannot be used for the detection of

Table 1
Summary of region-based techniques proposed in the literature.

#	Author (Year)	Approach	# Subjects	# Images	LD/IAD measurement	Performance Metrics	Limitations
1	Cinthio et al. [38]	Sub-pixel resolution method	NA	10 serial images of three phantoms	LD: Yes IAD: No	MD = 0.19, 0.04 and 0.37 μm	i. Under estimation of LD ii. Does not take care of tortuous or tilted arteries
2	Sifakis et al. [36]	Combination of anatomical knowledge and statistic	100	2149	No	NA	Relatively low performance in cases: i. Presence of carotid artery mimicking structure ii. Poor far wall visibility iii. An abruptly curved arterial shape iv. non-uniform luminal intensity
3	Rocha et al. [37]	Gaussian filtering and dynamic programming	25	199	No	NA	i. The near wall was not considered in the segmentation due to poor visibility ii. Fails in images with strong noise inside the CCA lumen region
4	Araki et al. [40]	Scale-space combined with pixel classification	202	404	LD: Yes IAD: No	CC: 0.92 POM: 98.0%	i. Need to be tested on high curved vessels
5	Kumar et al. [39]	Scale-space, spatial transformation and pixel classification	202	404	LD: Yes IAD: Yes	CC (LD):0.99 CC (IAD): 0.94 POM (LD):98.7% POM (IAD): 98.1%	i. Need to be tested on multi-ethnic data

MD: Mean Difference, CC: Coefficient of Correlation, POM: Precision of Merit, NA: Not Applicable

near MA wall due to poor visibility and hence difficult to adapt for the carotid LD estimation.

Araki et al. [40] used a region-based model to capture the lumen intensities under the constant blood density assumption. The ROI region is first captured using the combination of scale-space with vertical profile analysis. The ROI is then categorized into three different classes: (a) low intensity lumen region, (b) high intensity or brightest adventitia region and (c) medium intensity plaque region. For this reason, Araki et al. [40] adapted K-mean classifier with three pre-defined classes to separate the lumen region. Finally, the LD is estimated using the Polyline distance metric. Recently, Kumar et al. [39] modified the scale-space approach in [40] by including a spatial transformation based iterative step for the measurement of image-based LD and IAD in curved vessels. In this iterative procedure, the LD measurement is performed in the transformed image and the results are inverse transformed to the original image framework. The transformation consists of selecting L pixels above and below the lumen axis and creating a sub image. This approach can overcome the limitations of the existing methods that require the image interfaces to be horizontal at the time of acquisition. Further, the authors have included a non-local mean based denoising step in the overall pipeline which provided robustness to the system. Moreover, since the method presented in [39] is capable of measuring both LD and IAD simultaneously, the stroke risk evaluation in atherosclerotic cases can become more accurate. This is because both LD and IAD together turn out to be a more relevant biomarker for stroke risk prediction than LD alone [95]. Further in [39], the authors have used the same database as in [40] to test their algorithm and got improved results (refer Table 1).

2.1.4. Boundary-based techniques

The simplest approach for tracking the carotid wall borders is to use an edge detection technique which represents discontinuities in brightness or pixel intensity. However, the boundaries identified by edge detection techniques are often disconnected and one needs to find closed region boundaries for successful segmentation. Hence, some pre-processing techniques often apply prior to the segmentation in order to enhance the edges. Many methods were proposed in the literature for the detection of edges corresponding to the carotid artery interfaces which are summarized in Table 2.

Hough's transform was used for the automated carotid lumen segmentation in Golemati et al. [42]. Their assumption of straight lines (longitudinal images) and circles (transverse images) for carotid lumen received much attention among the research community. Due to changes in the shape and orientation of the carotid arteries during the acquisition protocol, it puts a challenge on the above assumptions in case of diseased carotid arteries. However, a solution is suggested by the authors to make use of active contours along with Hough's transform. Molinari et al. [44] used an integrated approach in order to extract the carotid artery layer. The method involves three steps, geometric feature extraction, line fitting, and classification, to produce the tracings of the proximal and distal adventitia layers. However, the deeper plaques protruding into the arterial lumen puts a challenge on the perfect delineation of adventitial borders. Moreover, the authors

Table 2
Summary of boundary-based (edge-based) techniques proposed in the literature.

#	Author	Approach	# subjects	# images	LD/IAD Measurement	Performance Metrics	Limitations
1	Golemati et al. [42]	Hough Transform	10	Image seq. of length 70–80	LD: Yes IAD: No	ACC: 98%	i. Fails if the arterial boundary has a random shape or curvature ii. Presence of speckle noise iii. Presence of thick plaque
2	Molinari et al. [44]	Integrated approach consisting of geometric feature extraction, line fitting, and classification	130	200	No	NA	Non-perfect tracing of boundaries in case of noisy lumen and overlap of the Jugular Vein (JV)
3	Rocha et al. [45]	RANSAC and cubic splines	25	50	No	NA	i. The amount of smoothing must be controlled ii. Misdetections of the carotid adventitia occur in presence of other similar structures
4	Rocha et al. [46]	Fuzzy classification	25	50	No	NA	Misdetections occur when similar boundaries are present
5	Santos et al. [41]	Chan-Vese level set segmentation model	–	11	No	NA	i. Fails if carotid artery image is of low contrast and noisy ii. Tested on a small database
6	Loizou et al. [43]	Snake based segmentation approach	20	20	LD: Yes IAD: No	CC: 0.63	i. Faces challenge of initialization of snakes ii. Only a small number of subjects included
7	Araki et al. [40]	Scale-space combined with level set	202	404	LD: Yes IAD: No	CC: 0.86 POM: 95.3%	Fails in case of an abruptly curved arterial shape

ACC: Accuracy, CC: Coefficient of Correlation, POM: Precision of Merit, NA: Not Applicable

have identified a repeated pattern of lumen walls due to the presence of other similar structures such as JV, under which the algorithm fails in the classification adventitial borders.

In Rocha et al. [45], random sample consensus (RANSAC) method is used for the semi-automatic segmentation of far and near adventitia boundaries of the CCA. The RANSAC search finds the best fit of a given contour model (which is evaluated according to a gain function). However, in some cases the thick plaque region pushes the lumen boundary away from the adventitia boundary. This can badly influences the effectiveness of the gain function resulting in under estimation and causes an increase in the number of samples analyzed by the RANSAC algorithm. In another approach proposed by Rocha et al. [46], a fuzzy classification method is used for the automated segmentation of carotid arteries to compute the lumen axis. Using fuzzy edge detection and feature extraction, all step and valley edges in the ROI are classified. Due to fragmented edges caused by echo attenuation and speckle, they are further refined and connected by using a DP algorithm which uses a fuzzy gain function. By adopting a fuzzy classifier, the authors have avoided the use of low pass filtering which might eliminate important weak edges. The major advantage of this method is that both the near and far wall boundaries were detected which is a pre-requisite for the LD/IAD computation, but the authors did not attempt.

In Santos et al. [41], the lumen and bifurcation contours are segmented using the Chan-vese (CV) level set segmentation [51] model along with morphologic operators. This threshold-based region detection is seldom susceptible to false region estimation if the images are noisy due to low resolution or hyperechoic characteristics or shadows due to the presence of calcium in the near wall. Further, the morphological operations are sensitive to noise and hence are not very stable [52]. Loizou et al. [43] introduced a 'Snake' based segmentation technique for the carotid bifurcation and diameter estimation. The 'Snake' should be initialized manually. However, since the propagation force is frequently based on intensity gradients, it makes the 'Snake' vulnerable to false edges and can sometimes leak through the discontinuities in the wall borders where the gradient is too weak [53–56].

Araki et al. [40] proposed a method that combines the scale-space paradigm with level set. In scale-space approach, image segmentations are computed at multiple scales. The general DRLSE (Distance Regularized Level set Evolution) technique proposed by Li et al. [57] is used for capturing the lumen edges within the ROI. The key advantage of using level set is that it has the ability to follow morphologic edges of the interfaces. Hough's transform is used as an initialization step before applying level set and is used to approximate the lumen borders using straight lines. The Hough's

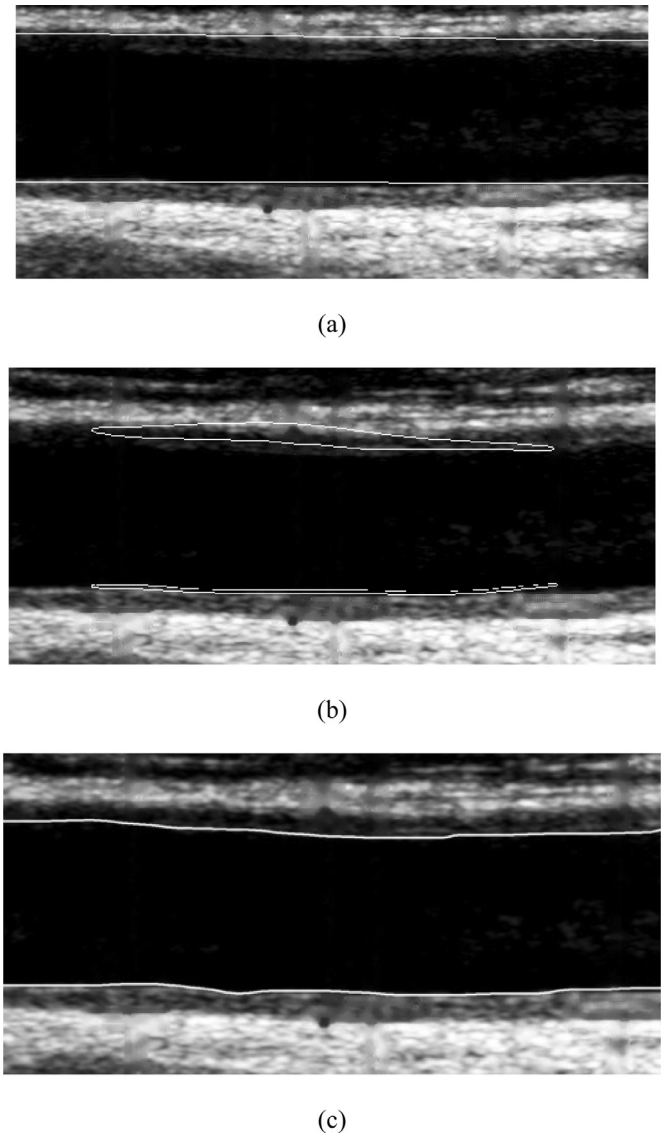

Fig. 6. Visual comparison of lumen segmentation algorithms on a single image (LI borders). (a) Hough's transform by Golemati et al. [42]; (b) Snake segmentation by Loizou et al. [43]; (c) Scale-space and region-based segmentation by Araki et al. [40].

transform will give small line segments which will constitute the boundary for the level set to explore.

In Fig. 6, visual comparison of lumen segmentation algorithms (to find LI borders) is illustrated on a single image. Fig. 6(a) showing the Hough's transform technique proposed in [42]. It can be seen that the straight line approximation is not suitable for segmenting the LI borders, as the vessel orientation cannot be expected as straight always. Further, we can notice a staircase effect appearing in the LI borders while trying to combine the different straight line segments. In Fig. 6(b), the 'Snake' segmentation technique in [43] is illustrated, where the points are converging at some other location rather than the actual contours (LI borders). This is due to the poor contrast of the carotid walls and presence of speckle and plaque content inside the lumen. Fig. 6(c), illustrates the region-based scale-space method proposed in [40], which is getting closer to the actual LI borders.

Even though, we have found more boundary-based approaches than region-based approaches in the literature, the region-based strategy is giving more satisfactory results when comparing the overall performance. This can be justified by considering the dependency of boundary-based algorithms on edges or image gradients. One explanation is that boundary-based methods are more sensitive to changes in gradient information at the wall borders during the cardiac cycle. The rapid changes in the velocity of blood flow in the artery causes subtle changes in the shape and size of lumen [58]. Since the image acquisition takes place during the cardiac cycle, it is often sensitive to these changes when the image frame gets frozen. One way to compensate for this sensitivity is to consider the neighboring frames. The second explanation for higher error is associated with the multi-focal nature of atherosclerotic disease. The random deposit of plaques along the carotid artery subsequently affects the intensity distribution and thickness of the diseased arterial wall. Further, boundary-based techniques are sensitive to sudden changes in the variations of the grayscale intensity distribution along the CCA, and will therefore yield less optimal results. This can be compensated for by taking regional statistics embedded with boundary-based information.

2.2. Challenges during CCA segmentation

A fully automated system for CCA segmentation from US images is an important requirement for physicians and vascular radiologists [59]. One should take the advantage of the knowledge in US image reconstruction in the segmentation process. Fig. 7 illustrates the dissimilarity in the carotid artery images in a database. The patients may have scanned with different hardware settings (frequency, depth, gain, etc.) and different positioning of probe which can affect the quality of image data. The LI and plaque borders generally have a very low contrast which makes it more difficult to capture [60]. Moreover, certain characteristic artifacts can cause difficulty in the segmentation task [42]. This includes signal attenuation and dropout, speckle noise and acoustic shadowing. The different challenges of CCA segmentation reported by different authors are reviewed in Table 3.

In US images, attenuation is the reduction in amplitude of the ultrasound beam as a function of distance through the imaging medium. Accounting for attenuation effects in ultrasound is important because reduced signal amplitude can affect the quality of the image produced [61]. Acoustic shadowing on an US image is characterised by a signal void behind structures that strongly absorb or reflect ultrasonic waves [62]. This happens most frequently with solid structures, as sound conducts most rapidly in areas where molecules are closely packed, such as in bone or stones. The direct effect of acoustic shadowing or echo attenuations in the segmentation task is that some boundary segments may be missing which may lead to edge leaking at the near and far LI interfaces (see Fig. 7).

Sensitivity to ultrasound vibrations at each depth of the body is different due to which the imaging suffer from signal loss from deeper in the tissue. Signal drop-out may occur frequently while imaging arteries with 65–70% stenosis, especially if the CCA is deposited with high amount of calcium [63]. This makes it difficult to determine the boundaries of the true lumen. US images are often considered as the hardest to segment among medical images due to their low signal to noise ratio (SNR) [64]. The presence of multiplicative speckle noise in carotid US images tends to reduce the image resolution and contrast thereby degrading the image quality. In some cases, due to increased speckle content, the segmentation algorithm may not be able to distinguish between carotid lumen and hypoechoic plaque tissue. There are many methods available for speckle noise reduction in the literature [65–67].

There are certain characteristics that make an US image suitable for automated delineation of carotid artery borders. These include high spatial resolution, high dynamic range, low noise level, compound and harmonic imaging [68]. Specific image enhancement or

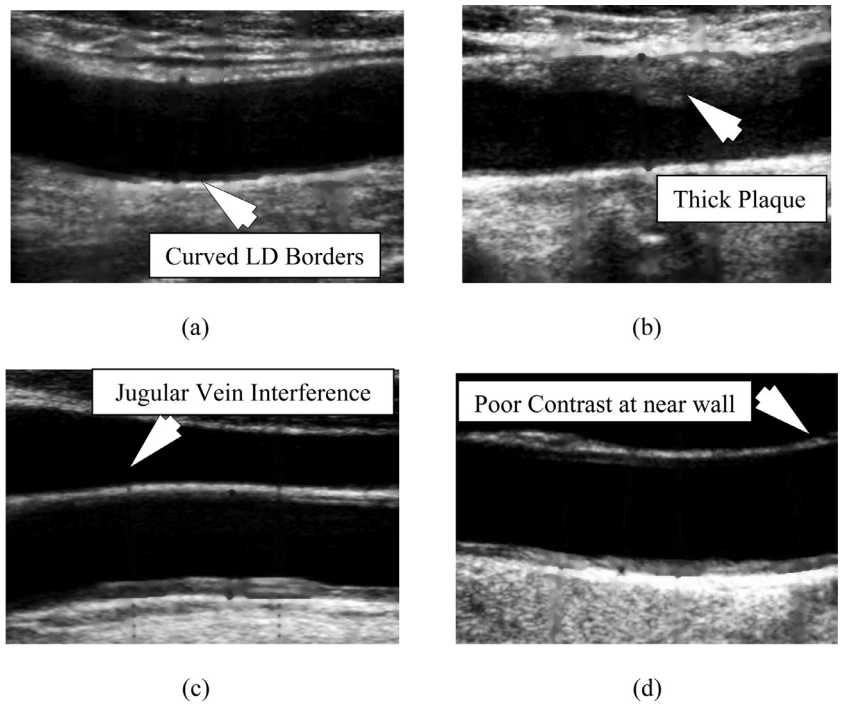

Fig. 7. Illustrating the variation of carotid artery images across different patients. (a) Curved lumen borders; (b) High plaque deposit and narrowing of carotid artery; (c) Low contrast image with jugular vein interference. (d) Image having poor contrast difference at near wall.

denoising strategies may need to be adopted, if the image does not possess these characteristics. The compound and harmonic imaging facility are available on most of the medium-level and high-level ultrasound OEM scanners, whereas they are not present in the majority of the entry-level and cheaper equipments. This results in a poor quality image with low contrast at the near and far LI interfaces leading to inaccurate segmentation.

The important factor that complicates the automatic detection of CCA is the presence of jugular vein (JV) structure which is often seen just above the CCA (see Fig. 7(c)). Since the echographic appearance of CCA and JV are very much similar, the near wall of the CCA can easily be confounded with the far boundary of the JV. Deeper plaques protruding into the carotid artery lumen represent another cause of imperfect segmentation. The plaque substantially perturbs the average intensity level of the CCA lumen. Usually, in patients with severe stenosis (>80%), hypoechoic plaques appear at both the walls [69]. This not only causes non-uniform luminal intensity, but also results in an abruptly curved arterial shape (e.g. due to a relatively large plaque). Therefore, the final boundary segmentation may have many deficiencies. Another major limitation of the existing algorithms is in the case of tortuous or tilted arteries. In these cases, since the artery is not horizontally scanned, a lateral averaging may result in an underestimation of the true lumen diameter.

2.3. Quantitative assessment of lumen segmentation systems

An automated carotid artery lumen segmentation system can be evaluated in two ways. One is by simple visual inspection of fine details which is only possible by expert physicians. The second way is to analyse the system quantitatively using some metric and compare the automated measurement against manual expert tracings, which are considered to be the ground truth (GT). Further, it is mandatory for an automated medical system to compare and validate against manual tracing in order to be accepted in the clinical domain. The following are some of the popular performance metrics found in the literature.

2.3.1. Coefficient of correlation (r)

The Pearson (linear) correlation coefficient (r) [70] measures the strength and the direction of a linear relationship between two variables (auto and manual measurements). The mathematical formula for computing r is [70]:

$$r = \frac{n\sum xy - (\sum x)(\sum y)}{\sqrt{n\left(\sum x^2\right) - (\sum x)^2}\sqrt{n\left(\sum y^2\right) - (\sum y)^2}} \tag{1}$$

Where n is the number of pairs of data, x and y are the variables of interest. The value of r is such that $-1 < r < +1$. The + and – signs are used for positive linear correlations and negative linear correlations, respectively. The standard method used to measure the 'significance' of this correlation analyses is the p-value. Typically, values of either 0.01 or 0.05 are taken as cutoff.

2.3.2. Coefficient of variation (CV)

The coefficient of variation (CV) can be calculated according to the formula [71]:

$$CV = \frac{S * 100}{\bar{x}} \tag{2}$$

where

$$S = \frac{SD}{\sqrt{2}} \tag{3}$$

$\bar{x}$ is the pooled mean and SD is the standard deviation for the difference between automated and manual measurements of LD.

2.3.3. Mean absolute distance (MAD)

Mean Absolute Distance (MAD) is used as a boundary distance-based metric. The averages of MAD can be computed using all vessels in the database images to obtain an overall estimate of boundary disagreement. The formula to compute MAD is given by [71]:

$$MAD_{M,T} = \frac{1}{K}\sum_{i=1}^{K} |d(m_i, a_i)| \tag{4}$$

Table 3
Important assumptions and challenges reported by different authors in the literature.

#	Author	Assumptions made	Challenges Reported
1	Golemati et al. [42]	Straight lines and circles were used to approximate the wall-lumen boundary	Speckle noise, acoustic shadowing, signal dropout, low contrast, curvature of arteries
2	Molinari et al. [44]	i. The artery should occupy the whole image frame width ii. Considered the artery structure as a region with low intensity (the lumen) surrounded by two bright stripes	Presence of jugular vein above the CCA, deeper plaques protruding into the artery lumen
3	Cinthio et al. [38]	Horizontal orientation for carotid artery	Tortuous or tilted arteries
4	Rocha et al. [45]	i. Carotid adventitia have valley-shaped intensity profile separated by a hypoechogenic region (media layer) ii. Cubic spline model for the adventitia boundary	Missing edges in carotid boundaries, occlusions caused by plaques, unpredictable bending of vessel along its major axis, variability in the artery shape
5	Rocha et al. [46]	Three class assumption: (i) dark objects (hypoechogenic tissues like blood); (ii) bright objects, like letters or graphical markings; and (iii) objects with intermediate brightness (echogenic tissues)	Low signal to noise ratio (SNR), artifacts like echo reverberations introduce false boundaries, acoustic shadowing or echo attenuations
6	Santos et al. [41]	Pixels belonging to the lumen region of the carotid artery are characterized by both low mean and standard deviation	Low contrast, speckle noise, gaps in the vessel boundaries, variability of its shape among subjects
7	Loizou et al. [43]	–	Speckle noise
8	Sifakis et al. [36]	i. Carotid artery located in the center of the image ii. From the bottom of the image and moving upwards, one ordinarily encounters the (usually brightest) far wall region, then the (usually darkest) lumen, and then the (usually second brightest) near wall	Appearance of carotid artery mimicking patterns at different depth ranges, varying luminal gray level, different arterial inclinations, presence of hypoechoic plaques, speckle noise
9	Rocha et al. [37]	i. Blood vessels appear as dark longitudinal regions (vessel lumen) surrounded by two bright boundaries (vessel walls) ii. CCA is larger than jugular vein (JV) and appears below JV.	Speckle noise, presence of other similar anatomical structures, partial missing of far wall region due to echo shadowing caused by calcified tissues
10	Araki et al. [40]	i. Distal (far) wall of the carotid artery has the brightest region ii. Constant blood density assumption	Variation in shape and size, occlusions caused by multi-focal plaques, arterial curvature, gaps within luminal borders, JV interference, poor contrast at near wall
11	Kumar et al. [39]	i. Distal (far) wall of the carotid artery has the brightest region ii. Constant blood density assumption iii. Curved vessels	Variation in shape and size, occlusions caused by multi-focal plaques, arterial curvature, gaps within luminal borders, JV interference, poor contrast at near wall, speckle noise level

where $d(m_i,a_i)$ is the distance between the boundary point m_i of the manual drawn contour and its corresponding boundary point on automated contour a_i, and K is the number of points included in the two boundaries (manual and automated). In the case where the two boundaries do not have the same number of points, then one of them can be interpolated. However, if the boundaries include curved segments, the MAD will be overestimated.

2.3.4. Precision of merit (PoM)

The overall system's performance was computed using the first method of precision-of-merit (PoM1) in percentage as [72]:

$$PoM1_{LD}\ (\%) = 100 - \left[\left(\frac{\left|\overline{LD}_{Auto} - \overline{LD}_{Manual}\right|}{\overline{LD}_{Manual}}\right) * 100\right] \tag{5}$$

where,

$$\overline{LD}_{Auto} = \frac{1}{N}\sum_{i=1}^{N} LD_{Auto_i}, \tag{6}$$

$$\overline{LD}_{Manual} = \frac{1}{N}\sum_{i=1}^{N} LD_{Manual_i} \tag{7}$$

LD_{Auto_i} is the measured automated lumen diameter and LD_{Manual_i} is the measured manual lumen diameter of a particular image. N is the total number of images in the database. This is a key feature that evaluates the automatically traced diameter difference compared to the manual diameter difference. Second method of precision of merit (PoM2) computation was using error difference between the automated and manual methods for each individual case (PoM per image). This is mathematically expressed as [73]:

$$PoM2_{LD}\ (\%) = 100 - \left[\frac{\sum_{i=1}^{N} \frac{|(LD_{Auto_i} - LD_{Manual_i})|}{LD_{Manual_i}}}{N}\right] * 100$$

2.3.5. Dice similarity and Jaccard Index

Dice similarity (DSC) and Jaccard index (JI) [74,75] were computed to find the similarity between two regions. Assume region A represents the area enveloped by the automated segmentation and region B represents the area enveloped using manual tracings. Then, DSC is the ratio of area in common to both region A and region B to the average size of region A and region B [74].

$$DSC = 200 \times \left(\frac{A \cap B}{A + B}\right) \tag{8}$$

Although very similar to Dice, JI shows the ratio of area in common to both region A and B to the total size of region A and B available [75].

$$JI = \left(\frac{A \cap B}{(A + B) - (A \cap B)}\right) \times 100 \tag{9}$$

Another possible way for comparison between automatically and manually segmented structures is by receiver operating characteristic (ROC) analysis [42], which assesses the specificity and sensitivity of the segmentation methods. Further, the regression plots can be used to show the variability between auto and manual tracings which is seen by the deviation from a trend line. Generally, this is a line of best fit through the data of two variables, and the Pearson correlation coefficient (r) indicates how far away all these data points are to this line of best fit. The Bland-Altman (BA) plot can demonstrate the level of agreement between two methods when measuring the same variable [76].

Different statistical tests can be used for the evaluation of the performance of the automated system against manual tracings. The statistical tests can be used to check the agreement between true and measured value of a variable. This is important since one algorithm may perform best in terms of bias, but a different algorithm may perform best in terms of precision. Often, the algorithm that has the best agreement with ground truth (GT) is considered to have the best performance. Due to this trade-off, the best performing algorithm (agrees best with ground truth) is not necessarily the best in terms of bias or precision. Use of statistical tests can do some help here, but we need to select the proper parameter (test statistic) that we want to test for agreement. For example, both the ANOVA test [77] and Chi-Square test [78] are used to analyze whether there exist a significant difference between the observed data (automated measurements) and the expected data (manual measurements or GT). However, the test statistics are different. Student's t test is often used to find whether the (strong and highly significant) correlation can be regarded as equality or not. In addition to this, different non-parametric statistical tests are used for testing the difference between several related samples [39,40]. For example, the Friedman test [79] is useful to find whether the sample medians are significantly different from each other. Mann-Whitney test [80] is another non-parametric test performed to determine whether or not two samples come from the same population. Usually in all the above tests, p-values less than 0.05 will be considered as statistically significant unless otherwise specified.

3. Results

3.1. Clinical significance of carotid LD and IAD

Non-invasive assessment of carotid arterial wall thickness using high-resolution US is often used in clinical trials as a surrogate marker of cardiovascular diseases. However, we believe that the carotid LD and IAD together has the potential to become a biomarker of stroke risk. In patients with significantly high volume of plaque which causes luminal narrowing, LD will be smaller. Hence, LD is inversely related to stenosis severity. As a result, as LD decreases, it seems reasonable to believe that there may be a resultant increased risk of ischemic stroke. Both the European Carotid Surgery Trial (ECST) [81] and the North American Symptomatic Carotid Endarterectomy Trial (NASCET) [82] indicate that the degree of stenosis can be expressed as a percentage reduction in vessel diameter. As discussed by Fox et al. [83], stenosis severity is calculated using the ratio of narrowed diameter at stenosis area to normal diameter in carotid artery. If LD_{narrow} is the measured lumen diameter of the arterial zone with maximum stenosis and LD_{normal} is the measured normal lumen diameter of the artery, then, stenosis severity index (SSI) [84] in percentage can be formulated as [83]:

$$SSI = \left(1 - \frac{LD_{narrow}}{LD_{normal}}\right) * 100 \tag{10}$$

The plaque growth leads to a compensatory arterial remodeling which is bidirectional in nature depending on the changes in the shear stress. While the positive remodeling results in an expansion of the arteries, negative remodeling may lead to an arterial narrowing [85]. An increase in the wall shear stress or decrease in the lumen area can lead to a dilation of the arterial wall for the normalization of the shear stress [86]. The severity of lumen narrowing of atherosclerotic arteries depends on the extent of the accumulation of plaque along the arterial wall. During the initial stages of atherosclerosis, compensatory enlargement of the artery is predominant. This results in an increase in the LD. However, when plaque occupies 30–40% of the vessel area, this adaptive mechanism fails. Further, the inflammatory changes and fibrosis may lead to constriction of the arterial wall, leading to augmentation of the lumen narrowing [87,88]. Meanwhile, the plaque growth causes the adventitia region to bulge up according to the Glagov phenomenon [89], which causes the IAD to increase. Due to this positive remodeling, the relationship between LD and IAD is important to consider and together may be useful imaging biomarkers for stroke risk stratification. The advantage of using LD/IAD as an imaging biomarker is its ability to provide reliable, accurate and highly reproducible measurements.

One of the key implications of LD/IAD measurement is to understand their correlation with other cardiovascular risk factors. The large size and ease of access by different imaging techniques makes the carotid artery an ideal potential surrogate for coronary artery disease (CAD) [90]. Recent studies have shown that carotid arterial diameters have a better predictive power for CAD [91]. It is known that the risk factors for both the carotid and coronary artery disease are similar [92–94]. Most recently Saba et al. [95] has performed a correlation study in CCA and has observed that the IAD is more strongly correlated to plaque score compared to carotid LD. Hence, this study suggests that carotid IAD may be a significant independent predictor of stroke risk along with traditional risk factors. Moreover, a study by Polak et al. [96] found that there exist a positive correlation between the carotid IAD and the incident stroke. They further suggested IAD as a stronger predictor of ischemic stroke in comparison to IMT.

3.2. Quantification of stenosis and risk assessment

Degree of carotid artery stenosis is an important risk factor for stroke. The ECST and the NASCET criteria have demonstrated that the risk of stroke is reduced by surgery in patients with high grade stenosis (70–99%). However, because the two trials used different methods to measure stenosis, the results are not comparable and the level of stenosis which is associated with increased risk of stroke cannot be strictly defined.

We have proposed a novel method in this study for quantification of stenosis and patient risk assessment based on carotid LD. Four different parameters were taken into consideration while computing the stroke risk. They are average LD value, minimum LD value, percentage stenosis severity index (SSI) and number of bumps in the LD value along the artery. The computation is straightforward as initially we need to find the score for each of the parameters based on the conditions given in the Table 4. Then the sum of these scores will be calculated for every single patient which will be used for computing the percentage risk index. Since the maximum score for a parameter is 5 and four parameters were computed for a patient, the maximum sum for any patient's image can be 20.

Percentage risk can then be computed according to the formula:

$$\text{Risk Index } (\%) = \left(\frac{\text{Sum of the scores}}{\text{Total score}}\right) * 100 \tag{11}$$

Table 4
LD severity conditions for different parameters for computing risk index.

Parameters	LD severity conditions	Score
Average LD	LD < 4 mm	5
	4 mm <= LD < 5 mm	4
	5 mm <= LD < 5 mm	3
	6 mm <= LD < 7 mm	2
	7 mm <= LD < 8 mm	1
	LD >= 8 mm	0
Minimum LD	LD < 3.5 mm	5
	3.5 mm <= LD < 4.5 mm	4
	4.5 mm <= LD < 5.5 mm	3
	5.5 mm <= LD < 6.5 mm	2
	6.5 mm <= LD < 7.5 mm	1
	LD >= 7.5 mm	0
Stenosis	Stenosis >= 50%	5
	40% <= Stenosis < 50%	4
	30% <= Stenosis < 40%	3
	20% <= Stenosis < 30%	2
	10% <= Stenosis < 20%	1
	Stenosis < 10%	0
# Bumps in LD value	Number of Bumps >= 5	5
	Number of Bumps = 4	4
	Number of Bumps = 3	3
	Number of Bumps = 2	2
	Number of Bumps = 1	1
	Number of Bumps = 0	0

Table 5
Patient risk percentage.

Risk Category	Condition	# Patients	% Patients
High risk	Risk Index > 66%	12	6
Moderate risk	33% < Risk Index <= 66%	84	41
Low risk	Risk Index <= 33%	107	53
Total		203	100

The result of this analysis on a patient database containing 203 patients is given in Table 5. In this database, 9 patients were identified as high risk patients, whereas 27 patients were identified as moderate risk patients. Remaining was considered as low risk patients.

4. Discussion

Computer assisted techniques have improved the accuracy and precision of carotid artery segmentation compared to the manual measurements. However, In order to completely analyze the progression or regression of atherosclerosis disease in patients, it is required to measure the changes in arterial diameters over time to time. This in turn makes it necessary to replicate the carotid artery examinations. Hence, the carotid US acquisition must be accurate and reproducible in both time and space. Since the US imaging is in real-time, the trained operator is able to adjust the scanning parameters such as: focusing, scanning depth, greyscale appearance, and time-gain compensation in order to have full control over the scanner [97]. Further, standardized positioning procedures assist in minimizing the changes. However, a patient's position on the examination table can rarely be reproduced exactly in different examinations. Counting this along with instrumental variability, it is difficult to obtain identical images in different scans. This point out the need for a universal standard by which carotid artery images can be acquired and arterial dimensions can be measured in an accurate and reproducible format. Further, we need to develop techniques which are scanner independent. Only a few techniques were addressed the issue of scanner independence before. Loizou et al. [43] have done a brightness adjustment of US images by normalizing them before further processing. This improves image compatibility by reducing the variability introduced by different gain settings, different operators, different equipment, and facilities [98]. However, normalization requires human interaction, since the operator has to choose the proper region for intensity remapping.

From Table 3, we have seen major challenges of CCA segmentation reported by different authors. So far, researchers have made several assumptions to tackle these challenges. In US images, the far wall of the carotid artery usually appears much brighter than the remaining regions [39]. This point can be used to reduce the complexity of the segmentation algorithms. The three class assumption for lumen region in [39,40,46] helps to deal with non-uniform plaques in the lumen. In [45], carotid adventitia is assumed to have valley-shaped intensity profile separated by a hypoechogenic region (media layer). In order to avoid the chances of misinterpretation of JV as carotid artery, an assumption has been made [36] to take up the order in which the structures are appearing i.e. from the bottom of the image and moving upwards, one ordinarily encounters the (usually brightest) far wall region, then the (usually darkest) lumen, and then the (usually second brightest) near wall.

4.1. Importance of multi-ethnic and different OEM data collection

In order to prove the applicability of automated segmentation systems in clinical practice, they must be sufficiently tested in multi-centric studies with multi original equipment manufacturer (OEM) data [99]. The important point to note here is that the quality of carotid US images is often decided by the sonographer. In a multi-centric study, the images will be acquired by different sonographers whose training or experience varies. This will produce a database which contains images of different quality. Further, the intra-sonographer variability during the examination period can be assessed from the data obtained by repeating complete carotid US studies on a number of subjects. Experimental performance of the automated algorithms on different OEM datasets will help to assess the image quality which later enables OEMs and integrators to build better machines.

4.2. Need for an integrated system

Integrated systems are desirable for the clinical experts in order to evaluate the risk of stroke in a precise and efficient way both in asymptomatic and symptomatic subjects [100]. Here, integrated system means a system (software application) which is able to segment the carotid artery, measure the required parameter (LD/IAD/IMT), and stratify the atherosclerotic plaque based on that. Such a system should be able to exploit the morphological features of the artery wall. A standard integrated system for B-mode carotid US should have the following stages: normalization and despeckle filtering, segmentation, feature extraction and selection, and classification [101].

4.3. Carotid artery segmentation in GPU framework

One of the important issues regarding the modern segmentation algorithms is the computational cost. This results from different factors such as size of the image, number of sampling points and multi-resolution algorithms. For example, we need more number of samples to represent the boundary of a curved artery than in case of straight ones. Further, some algorithms use complex iterative steps to achieve high accuracy for the measurement [102]. This in turn requires more processing power than conventional simple approaches which are straight forward. To avoid this limitation GPUs (graphics processing unit), can be utilized which provides excellent computing performance gain (up to 54 times faster than the parallel CPU implementation) [103].

4.4. Deep learning based systems

A general trend among all the state of the art methods is that they are making use of spatial techniques effectively, whereas cutting-edge statistical and machine-learning methods were not being fully utilized. Currently, deep learning (DL) is emerged as a serious contender in the field, winning many important machine learning competitions. The immense popularity of DL is because of higher performance in comparison with other conventional algorithms. The availability of GPUs and multi-core processor chips has made DL immensely popular among the research community. Accuracy of estimated LI and MA interfaces can be improved by DL. A combination of DL methods with the classical methods should be considered.

4.5. Arterial wall changes during the cardiac cycle

The study of dynamic properties of the carotid artery wall is becoming more common, since its mechanical and structural properties can change before the occurrence of clinical symptoms of cardiovascular diseases [104]. Arterial stiffness indices can be estimated by measuring arterial diameter changes during the cardiac cycle [105,106]. There are techniques such as artery distensibility, strain imaging [107,108] or pulse wave velocity (PWV) [109, 110], which can give close values of arterial wall stiffness. Another technique is by recording the blood flow velocities of the carotid artery during the systolic and diastolic phases [111]. However, this requires pulsed Doppler imaging which requires special equipment and training available in only a few centers. Since the facility for acquiring B-mode US measurements of carotid artery diameters and plaque prevalence are already present in numerous study centers and radiology clinics, measurements of arterial stiffness from changes in diameter measurements could potentially provide useful additional end points. Nevertheless, this technique has gained little popularity and its clinical implications remains to be elucidated. Further, it can be observed that most of the previous studies were focused on the development of segmentation algorithms in still images, and the same cannot be used for video US data due to the lack of inter-frame correlation.

4.6. Role of carotid bulb lumen in quantification of stenosis

One of the disadvantages of the NASCET method is that it underestimates the size of the plaque in the carotid bulb. For example, a plaque that uniformly fills the bulb will produce a lumen measurement equal to the distal internal carotid artery (ICA). Therefore, it is equally important to measure the minimal residual lumen (at the point of tightest stenosis in the bulb or the proximal ICA) and the corresponding outer ICA or bulb diameters [112]. Moreover, artery bifurcations, junctions, and regions of high curvature (such as the bulb), are identified as the most probable sites for the atherosclerotic diseases to occur [113]. These elements together with the complex geometry of a residual lumen in a stenotic carotid bulb constitute a very risky zone, whose significance must be verified in a large clinical trial. Recently, an approach [114] is proposed to measure the segmental IMT (sIMT) proximal to the bulb edge. Since this approach is capable of delineating the LI and MA borders of both near and far carotid wall, it can be extended to measure the LD/IAD in carotid bulb region.

4.7. Standardization of validation process

Effective algorithm validation contributes significantly to assuring the quality of algorithm. Different authors have used different performance metrics on different data for validating their techniques. Hence, a direct comparison of LD/IAD measurement performance cannot be done. Standardization should be introduced in the validation process and performance metric adoption in order to ensure its deliverability. Further, there exist no public domain databases and no public GT available for validation purpose which may be counted as a limitation in the development stage.

Even though we tried to explain all the aspects of carotid artery segmentation, there are some topics which are not very relevant and could not be discussed in the scope of this work. Doppler color US was not part of this study; hence we did not take lumen segmentation using color Doppler into consideration. Second, this study was only focused on longitudinal carotid US images; hence transverse images were not inherently discussed. The current study focused on the characteristics of images which were static in nature, unlike cine loop imaging [115] where temporal information can be interfaced. This topic was left out in our current study. Our main focus in this model was to compare and contrast segmentation approaches applied to static imagery and risk assessment approaches. Since the performance metrics between different studies were modeled differently along with the input characteristics of the carotid US data sets, hence, one of the challenges to compare and contrast these techniques.

5. Conclusions

We have presented different techniques for the lumen segmentation of the CCA from B-mode US images and its measurement of LD/IAD. These techniques include Hough transform, geometrical approaches, local statistics based techniques, fuzzy classification, dynamic programing, active contour or snake based techniques, scale-space and level set segmentation. The use of computer-aided measurement techniques has the potential benefit of increased accuracy with less computational complexity and less subjectivity. It is expected that the performance of the automated methods will get further increased with the rapidly growing development of technology such as 3D carotid imaging [116] and video segmentation [117,118]. The major consideration in future will be more towards the development of completely automatic integrated systems. However, more validation studies will be required to establish the state-of-the-art on segmentation performance.

Conflict of interest

Dr. Jasjit S. Suri has a relationship with AtheroPoint™, Roseville, CA, USA which is dedicated to Atherosclerosis Disease Management including Stroke and Cardiovascular imaging.

Reference

[1] World-heart-federation. http://www.world-heart-federation.org/cardiovascular health/stroke/
[2] Stroke Statistics. Available at: www.strokecenter.org/patients/about-stroke/stroke-statistics/
[3] P. Sobieszczyk, J. Beckman, Carotid artery disease, Circulation 114 (2006) e244–e247.
[4] “What is a Stroke?”. www.nhlbi.nih.gov/health/health-topics/topics/stroke. June 22, 2016
[5] K. Sakakura, M. Nakano, F. Otsuka, et al., Pathophysiology of atherosclerosis plaque progression. Heart, Lung and Circulation 22 (2013) 399–411.
[6] C. dev Sahu, M. Wintermark, Multi-Modality Atherosclerosis Imaging and Diagnosis, Springer Science & Business Media (2014).
[7] N. Deshpande, A. Needles, J.K. Willmann, Molecular ultrasound imaging: current status and future directions, Clinical Radiology 65 (2010) 567–581.
[8] J.M. Sanches, A.F. Laine, J.S. Suri, Ultrasound Imaging: advances and applications, Springer Science & Business Media (2012).
[9] S. Sarkar, S. Ghosh, S.K. Ghosh, et al., Role of transcranial Doppler ultrasonography in stroke, Postgraduate Medical Journal 83 (2007) 683–689.
[10] C.C. Branas, M.S. Weingarten, M. Czeredarczuk, et al., Examination of carotid arteries with quantitative color Doppler flow imaging, Journal of Ultrasound in Medicine 13 (1994) 121–127.
[11] S. Mehra, Role of Duplex Doppler sonography in arterial stenoses, Journal Indian Academy of Clinical Medicine 11 (2010) 294–299.

[12] S.A. Jones, H. Leclerc, G.P. Chatzimavroudis, et al., The influence of acoustic impedance mismatch on poststenotic pulsed-doppler ultrasound measurements in a coronary artery model, Ultrasound in Medicine & Biology 22 (1996) 623–634.
[13] B.A. Carroll, Carotid sonography, Radiology 178 (1991) 303–313.
[14] J.H. Stein, C.E. Korcarz, R.T. Hurst, et al., Use of carotid ultrasound to identify subclinical vascular disease and evaluate cardiovascular disease risk: a consensus statement from the American Society of Echocardiography Carotid Intima-Media Thickness Task Force endorsed by the Society for Vascular Medicine, Journal of the American Society of Echocardiography 21 (2008) 93–111.
[15] J.F. Polak, Peripheral vascular sonography, Lippincott Williams & Wilkins, 2004.
[16] M.L. Eigenbrodt, R. Sukhija, K.M. Rose, et al., Common carotid artery wall thickness and external diameter as predictors of prevalent and incident cardiac events in a large population study, Cardiovascular Ultrasound 5 (2007) 1–11.
[17] M.L. Eigenbrodt, Z. Bursac, K.M. Rose, et al., Common carotid arterial inter adventitial distance (diameter) as an indicator of the damaging effects of age and atherosclerosis, a cross-sectional study of the Atherosclerosis Risk in Community Cohort Limited Access Data (ARICLAD), 1987–89, Cardiovascular Ultrasound 4 (2006) 1–10.
[18] J.F. Polak, R.A. Kronmal, G.S. Tell, et al., Compensatory increase in common carotid artery diameter: Relation to blood pressure and artery intima-media thickness in older adults, Cardiovascular Health Study. Stroke 27 (1996) 2012–2015.
[19] K. Jensen-Urstad, M. Jensen-Urstad, J. Johansson, Carotid artery diameter correlates with risk factors for cardiovascular disease in a population of 55-year-old subjects, Stroke 30 (1999) 1572–1576.
[20] J.F. Polak, R.L. Sacco, W.S. Post, et al., Incident Stroke Is Associated With Common Carotid Artery Diameter and Not Common Carotid Artery Intima-Media Thickness, Stroke 45 (2014) 1442–1446.
[21] J.F. Polak, Q. Wong, W.C. Johnson, et al., Associations of cardiovascular risk factors, carotid intima-media thickness and left ventricular mass with inter-adventitial diameters of the common carotid artery: the Multi-Ethnic Study of Atherosclerosis (MESA), Atherosclerosis 218 (2011) 344–349.
[22] M.M. Mughal, M.K. Khan, J.K. DeMarco, et al., Symptomatic and asymptomatic carotid artery plaque, Expert Review of Cardiovascular Therapy 9 (2011) 1315–1330.
[23] O.N. Roxana, A.P. Balanescu, D. Constantinescu, et al., Imaging atherosclerosis by carotid intima-media thickness in vivo: how to, where and in whom? Maedica 7 (2012) 153–162.
[24] J. Suri, C. Kathuria, F. Molinari (Eds.), Atherosclerosis disease management, Springer Science & Business Media, 2010.
[25] A. Nicolaides, K.W. Beach, E. Kyriacou, et al., Ultrasound and carotid bifurcation atherosclerosis, Springer Science & Business Media (2011).
[26] L. Saba, R. Montisci, F. Molinari, et al., Comparison between manual and automated analysis for the quantification of carotid wall by using sonography, A validation study with CT. European Journal of Radiology 81 (2012) 911–918.
[27] L. Saba, F. Molinari, K.M. Meiburger, et al., Inter-and intra-observer variability analysis of completely automated cIMT measurement software (AtheroEdge™) and its benchmarking against commercial ultrasound scanner and expert Readers, Computers in Biology and Medicine 43 (2013) 1261–1272.
[28] C.L. de Korte, H.H. Hansen, A.F. van der Steen, Vascular ultrasound for atherosclerosis imaging, Interface Focus 1 (2011) 565–575.
[29] N.D. Londhe, J.S. Suri, Superharmonic imaging for medical ultrasound: a review, Journal of Medical Systems 40 (2016) 1–16.
[30] J.M. Sanches, A.F. Laine, J.S. Suri, Ultrasound Imaging, Springer Science & Business Media, 2012.
[31] L. Saba, J.M. Sanches, L.M. Pedro, et al., Multi-modality atherosclerosis imaging and diagnosis, Springer Science & Business Media (2014).
[32] J.S. Suri, C. Yuan, D.L. Wilson, Plaque imaging: pixel to molecular level, 113, IOS Press, 2005.
[33] J.F. Polak, R.L. Sacco, W.S. Post, et al., Incident stroke Is associated with common carotid artery diameter and not common carotid artery intima-media thickness, Stroke 45 (2014) 1442–1446.
[34] K. Jensen-Urstad, M. Jensen-Urstad, J. Johansson, Carotid artery diameter correlates with risk factors for cardiovascular disease in a population of 55-year-old subjects, Stroke 30 (1999) 1572–1576.
[35] C. Godia E, R. Madhok, J. Pittman, et al., Carotid artery distensibility a reliability study, Journal of Ultrasound in Medicine 26 (2007) 1157–1165.
[36] E.G. Sifakis, S. Golemati, Robust carotid artery recognition in longitudinal B–mode ultrasound images, IEEE Transactions in Image Processing 23 (2014) 3762–3772.
[37] R. Rocha, J. Silva, A. Campilho, Automatic detection of the carotid lumen axis in B-mode ultrasound images, Computer Methods and Programs in Biomedicine 115 (2014) 110–118.
[38] M. Cinthio, T. Jansson, A. Eriksson, et al., Evaluation of an algorithm for arterial lumen diameter measurements by means of ultrasound, Medical & Biological Engineering & Computing 48 (2010) 1133–1140.
[39] P.K. Kumar, T. Araki, J. Rajan, et al., Accurate lumen diameter measurement in curved vessels in carotid ultrasound: an iterative scale-space and spatial transformation approach, Medical & Biological Engineering & Computing 55 (2017) 1415–1434.
[40] T. Araki, P.K. Kumar, H.S. Suri, et al., Two automated techniques for carotid lumen diameter measurement: regional versus boundary approaches, Journal of Medical Systems 40 (2016) 1–19.
[41] A.M.F. Santos, J.M.R.S. Tavares, L. Sousa, et al., Automatic segmentation of the lumen of the carotid artery in ultrasound B-mode images, Expert Systems with Applications 40 (2013) 6570–6579.
[42] S. Golemati, J. Stoitsis, E.G. Sifakis, et al., Using the Hough transform to segment ultrasound images of longitudinal and transverse sections of the carotid artery, Ultrasound in Medicine and Biology 33 (2007) 1918–1932.
[43] P. Loizou C, T. Kasparis, C. Spyrou, et al., Integrated system for the complete segmentation of the common carotid artery bifurcation in ultrasound images, Artificial Intelligence Applications and Innovations 412 (2013) 292–301.
[44] F. Molinari, G. Zeng, J.S. Suri, An integrated approach to computer based automated tracing and its validation for 200 common carotid arterial wall ultrasound images, Journal of Ultrasound in Medicine 29 (2010) 399–418.
[45] R. Rocha, A. Campilho, J. Silva, et al., Segmentation of ultrasound images of the carotid using RANSAC and cubic splines, Computer Methods and Programs in Biomedicine 101 (2011) 94–106.
[46] R. Rocha, J. Silva, A. Campilho, Automatic segmentation of carotid B-mode images using fuzzy classification, Medical & Biological Engineering & Computing 50 (2012) 533–545.
[47] M. Prosi, K. Perktold, H. Schima, Effect of continuous arterial blood flow in patients with rotary cardiac assist device on the washout of a stenosis wake in the carotid bifurcation: a computer simulation study, Journal of Biomechanics 40 (2007) 2236–2243.
[48] A. Mahalingam, U.U. Gawandalkar, G. Kini, et al., Numerical analysis of the effect of turbulence transition on the hemodynamic parameters in human coronary arteries, Cardiovascular Diagnosis and Therapy 6 (2016) 208–220.
[49] J.S. Suri, D. Wilson, S. Laxminarayan, Handbook of biomedical image analysis, 2, Springer Science & Business Media, 2005.
[50] A. El-Baz, X. Jiang, J.S. Suri (Eds.), Biomedical image segmentation: advances & trends, CRC Press, 2016.
[51] T.F. Chan, L.A. Vese, Active contours without edges, IEEE Transactions on Image Processing 10 (2001) 266–277.
[52] O. Sigmund, Morphology-based black and white filters for topology optimization, Structural and Multidisciplinary Optimization 33 (2007) 401–424.
[53] F. Molinari, K.M. Meiburger, L. Saba, et al., Fully automated dual-snake formulation for carotid intima-media thickness measurement a new approach, Journal of Ultrasound in Medicine 31 (2012) 1123–1136.
[54] J.S. Suri, K. Liu, S. Singh, et al., Shape recovery algorithms using level sets in 2-D/3-D medical imagery: a state-of-the-art review, IEEE Transactions on Information Technology in Biomedicine 6 (2002) 8–28.
[55] J.S. Suri, S. Laxminarayan, PDE and level sets, Springer Science & Business Media (2002).
[56] Giraldi G.A., Rodrigues P.S., Suri J.S. Implicit dual snakes for medical imaging. Proceedings of the Engineering in Medicine and Biology Society (EMBS' 06), New york, USA; IEEE 2006: 3025-3028.
[57] C. Li, C. Xu, C. Gui, et al., Distance regularized level set evolution and its application to image segmentation, IEEE Transactions on Image Processing 19 (2010) 3243–3254.
[58] T.Y. Chow, J.S. Cheung, Y. Wu, et al., Measurement of common carotid artery lumen dynamics during the cardiac cycle using magnetic resonance TrueFISP cine imaging, Journal of Magnetic Resonance Imaging 28 (2008) 1527–1532.
[59] F. Molinari, G. Zeng, J.S. Suri, A state of the art review on intima–media thickness (IMT) measurement and wall segmentation techniques for carotid ultrasound, Computer Methods and Programs in Biomedicine 100 (2010) 201–221.
[60] F. Molinari, G. Zeng, J.S. Suri, Inter-greedy technique for fusion of different segmentation strategies leading to high-performance carotid IMT measurement in ultrasound images, Journal of Medical Systems 35 (2011) 905–919.
[61] S.C. Bushong, Diagnostic Ultrasound: Essentials of Medical Imaging Series, McGraw-Hill/Appleton & Lange, 1999.
[62] J.L. Whittaker, Ultrasound imaging for rehabilitation of the lumbopelvic region: a clinical approach, Elsevier Health Sciences (2007).
[63] D.P. Slovut, J.M. Romero, K.M. Hannon, et al., Detection of common carotid artery stenosis using duplex ultrasonography: a validation study with computed tomographic angiography, Journal of Vascular Surgery 51 (2010) 65–70.
[64] P.S. Hiremath, P.T. Akkasaligar, S. Badiger, Speckle Noise Reduction in Medical Ultrasound Images, in: G. Gunarathne (Ed.), Advancements and Breakthroughs in Ultrasound Imaging. InTech, 2013, pp. 201–241.
[65] O.V. Michailovich, A. Tannenbaum, Despeckling of medical ultrasound images, IEEE Transactions on Ultrasonics, Ferroelectrics, and Frequency Control 53 (2006) 64–78.
[66] J. Zhang, G. Lin, L. Wu, et al., Wavelet and fast bilateral filter based de-speckling method for medical ultrasound images, Bio-medical Signal Processing and Control 18 (2015) 1–10.
[67] P.C. Tay, C.D. Garson, S.T. Acton, et al., Ultrasound despeckling for contrast enhancement, IEEE Transactions on Image Processing 19 (2010) 1847–1860.
[68] F. Molinari, K.M. Meiburger, G. Zeng, et al., Automated carotid IMT measurement and its validation in low contrast ultrasound database of 885 patient Indian population epidemiological study: results of AtheroEdge™ Software, International angiology 31 (2012) 42.
[69] J.F. Polak, L. Shemanski, D.H. O'Leary, et al., Hypoechoic plaque at US of the carotid artery: an independent risk factor for incident stroke in adults aged 65 years or older, Cardiovascular Health Study. Radiology 208 (1998) 649–654.
[70] M.J. Campbell, T.D.V. Swinscow, Statistics at square one, John Wiley & Sons, 2011.

[71] Q. Liang, I. Wendelhag, J. Wilkstrand, et al., A multiscale dynamic programming procedure for boundary detection in ultrasonic artery images, IEEE Transactions in Medical Imaging 19 (2002) 127–142.
[72] N. Ikeda, A. Gupta, N. Dey, et al., Improved correlation between carotid and coronary atherosclerosis SYNTAX score using automated ultrasound carotid bulb plaque IMT measurement, Ultrasound in Medicine & Biology 41 (2015) 1247–1262.
[73] J.S. Suri, R.M. Haralick, F.H. Sheehan, Greedy algorithm for error correction in automatically produced boundaries from low contrast ventriculograms, Pattern Analysis & Applications 3 (2000) 39–60.
[74] A. Bharatha, M. Hirose, N. Hata, et al., Evaluation of three-dimensional finite element-based deformable registration of pre-and intraoperative prostate imaging, Medical Physics 28 (2001) 2551–2560.
[75] P. Jaccard, The distribution of the flora in the alpine zone, New Phytologist 11 (1912) 37–50.
[76] J.M. Bland, D.G. Altman, Statistical methods for assessing agreement between two methods of clinical measurement, The lancet 327 (1986) 307–310.
[77] D. Howell, Statistical methods for psychology, Cengage Learning (2012).
[78] D.G. Altman, Practical statistics for medical research, Chapman and Hall, 1991.
[79] M. Hollander, D.A. Wolfe, E. Chicken, Non-parametric statistical methods, John Wiley & Sons, 2013.
[80] S. Jackson, Research methods and statistics: A critical thinking approach, Cengage Learning (2015).
[81] European carotid surgery trialists' collaborative group, MRC European carotid surgery trial: interim results for symptomatic patients with severe (70-99%) or with mild (0-29%) carotid stenosis, Lancet 337 (1991) 1235–1243.
[82] North American symptomatic carotid endarterectomy trial collaborators, Beneficial effect of carotid endarterectomy in symptomatic patients with high–grade carotid stenosis, New England Journal of Medicine 325 (1991) 445–453.
[83] A.J. Fox, How to measure carotid stenosis, Radiology 186 (1993) 316–318.
[84] T. Araki, A.M. Kumar, K.P. Kumar, et al., Ultrasound-based automated carotid lumen diameter/stenosis measurement and its validation system, Journal for Vascular Ultrasound 40 (2016) 120–134.
[85] M.R. Ward, G. Pasterkamp, A.C. Yeung, et al., Arterial remodeling mechanisms and clinical implications, Circulation 102 (2000) 1186–1191.
[86] A. Lafont, L.A. Guzman, P.L. Whitlow, et al., Restenosis after experimental angioplasty intimal, medial, and adventitial changes associated with constrictive remodeling, Circulation Research 76 (1995) 996–1002.
[87] D.W. Losordo, K. Rosenfield, J. Kaufman, et al., Focal compensatory enlargement of human arteries in response to progressive atherosclerosis, In vivo documentation using intravascular ultrasound. Circulation 89 (1994) 2570–2577.
[88] G. Pasterkamp, P.J.W. Wensing, M.J. Post, et al., Paradoxical arterial wall shrinkage may contribute to luminal narrowing of human atherosclerotic femoral arteries, Circulation 91 (1995) 1444–1449.
[89] S. Glagov, E. Weisenberg, C.K. Zarins, et al., Compensatory enlargement of human atherosclerotic coronary arteries, New England Journal of Medicine 316 (1987) 1371–1375.
[90] C. Yuan, N.L. Polissar, T.S. Hatsukami, What will noninvasive carotid atherosclerosis imaging show us about high-risk coronary plaques? Journal of the American College of Cardiology 58 (2011) 423–425.
[91] A.M. Mirek, A. Wolińska-Welcz, Is the lumen diameter of peripheral arteries a good marker of the extent of coronary atherosclerosis? Kardiologia Polska 71 (2012) 810–817.
[92] F. Jashari, P. Ibrahimi, R. Nicoll, et al., Coronary and carotid atherosclerosis: similarities and differences, Atherosclerosis 227 (2013) 193–200.
[93] T. Araki, N. Ikeda, F. Molinari, et al., Link between automated coronary calcium volumes from intravascular ultrasound to automated carotid IMT from B-mode ultrasound in coronary artery disease population, International Angiology 33 (2014) 392–403.
[94] J.R. Crouse, J.F. Toole, W.M. McKinney, et al., Risk factors for extracranial carotid artery atherosclerosis, Stroke 18 (1987) 990–996.
[95] L. Saba, T. Araki, K.P. Kumar, et al., Carotid inter-adventitial diameter is more strongly related to plaque score than lumen diameter: An automated tool for stroke analysis, Journal of Clinical Ultrasound 44 (2016) 210–220.
[96] J.F. Polak, R.L. Sacco, W.S. Post, et al., Incident stroke is associated with common carotid artery diameter and not common carotid artery intima-media thickness, Stroke 45 (2014) 1442–1446.
[97] D. Lee, Y.S. Kim, J.B. Ra, Automatic time gain compensation and dynamic range control in ultrasound imaging systems, Medical Imaging: Ultrasonic imaging and signal Processing 6147 (2006) 1–9.
[98] C.P. Loizou, C.S. Pattichis, M. Pantziaris, et al., Quality evaluation of ultrasound imaging in the carotid artery based on normalization and speckle reduction filtering, Medical and Biological Engineering and Computing 44 (2006) 414–426.
[99] F. Molinari, K.M. Meiburger, L. Saba, et al., Ultrasound IMT measurement on a multi-ethnic and multi-institutional database: our review and experience using four fully automated and one semi-automated methods, Computer Methods and Programs in Biomedicine 108 (2012) 946–960.
[100] H. Papadopoulos, A.S. Andreou, L.S. Iliadis, et al., Artificial Intelligence Applications and Innovations, in: Proceedings of the 9th IFIP WG 12.5 international conference, AIAI, Paphos, Cyprus, 2013.
[101] C.P. Loizou, M. Pantziaris, An integrated system for the complete segmentation of the common carotid artery bifurcation in ultrasound images, Journal of Biomedical Engineering and Informatics 1 (2015) p11.
[102] S.K. Setarehdan, S. Singh, Advanced algorithmic approaches to medical image segmentation: state-of-the-art applications in cardiology, neurology, mammography and pathology, Springer Science & Business Media, 2012.
[103] R. Narayanan, P.N. Werahera, A. Barqawi, et al., Adaptation of a 3D prostate cancer atlas for transrectal ultrasound guided target-specific biopsy, Physics in Medicine and Biology 53 (2008) N397.
[104] R.H. Selzer, W.J. Mack, P.L. Lee, et al., Improved common carotid elasticity and intima-media thickness measurements from computer analysis of sequential ultrasound frames, Atherosclerosis 154 (2001) 185–193.
[105] J.F. Polak, A. Meisner, M.J. Pencina, et al., Variations in common carotid artery intima-media thickness during the cardiac cycle: implications for cardiovascular risk assessment, Journal of the American Society of Echocardiography 25 (2012) 1023–1028.
[106] S. Graf, J. Gariepy, M. Massonneau, et al., Experimental and clinical validation of arterial diameter waveform and intimal media thickness obtained from B-mode ultrasound image processing, Ultrasound in Medicine & Biology 25 (1999) 1353–1363.
[107] G. Gamble, J. Zorn, G. Sanders, et al., Estimation of arterial stiffness, compliance, and distensibility from M-mode ultrasound measurements of the common carotid artery, Stroke 25 (1994) 11–16.
[108] A.K. Patel, H.S. Suri, J. Singh, et al., A review on atherosclerotic biology, wall stiffness, physics of elasticity, and its ultrasound-based measurement, Current Atherosclerosis Reports 18 (2016) 83.
[109] S. Laurent, J. Cockcroft, L. Van Bortel, et al., Expert consensus document on arterial stiffness: methodological issues and clinical applications, European Heart Journal 27 (2006) 2588–2605.
[110] T. Pereira, C. Correia, J. Cardoso, Novel methods for pulse wave velocity measurement, Journal of Medical and Biological Engineering 35 (2015) 555–565.
[111] H. Zachrisson, B. Berthelsen, C. Blomstrand, et al., High diastolic flow velocities in severe internal carotid artery stenosis: A sign of increased surgical risk? Journal of Vascular Surgery 31 (2000) 477–483.
[112] W.E. Shaalan, C.M. Wahlgren, T. Desai, et al., Reappraisal of velocity criteria for carotid bulb/internal carotid artery stenosis utilizing high-resolution B–mode ultrasound validated with computed tomography angiography, Journal of Vascular Surgery 48 (2008) 104–112.
[113] K.T. Nguyen, C.D. Clark, T.J. Chancellor, et al., Carotid geometry effects on blood flow and on risk for vascular disease, Journal of Biomechanics 41 (2008) 11–19.
[114] N. Ikeda, N. Dey, A. Sharma, et al., Automated segmental-IMT measurement in thin/thick plaque with bulb presence in carotid ultrasound from multiple scanners: Stroke risk assessment, Computer Methods and Programs in Biomedicine 141 (2017) 73–81.
[115] L. Gerrit, G. Renaud G, Z. Akkus, et al., Far-wall pseudo enhancement during contrast-enhanced ultrasound of the carotid arteries: clinical description and in vitro reproduction, Ultrasound in Medicine and Biology 38 (2012) 593–600.
[116] Tan C.L., Sinha R., Budohoski K., et al. MR Imaging of Vulnerable Carotid Atherosclerotic Plaques. In 3D Imaging Technologies in Atherosclerosis. Springer 2015: 171-186.
[117] N. Ikeda, T. Araki, N. Dey, et al., Automated and accurate carotid bulb detection, its verification and validation in low quality frozen frames and motion video, International Angiology 33 (2014) 573–589.
[118] S.K. Banchhor, T. Araki, N.D. Londhe, et al., Five multiresolution-based calcium volume measurement techniques from coronary IVUS videos: a comparative approach, Computer Methods and Programs in Biomedicine 134 (2016) 237–258.